

escape by thwarting thermal escape (17). If the early Archean thermopause (the top of the thermosphere or "exobase") were <500 K compared with today's temperature of ~1000 K, the thermal escape of H atoms at the thermopause would have been significantly lowered. However, this speculation does not stand up to scrutiny. Various species (N<sub>2</sub>, O<sub>2</sub>, H, and He) absorb UV radiation and warm the thermosphere. The Archean's lack of O<sub>2</sub> absorption would not cause a colder thermopause than today because extreme UV fluxes (EUV) from the Archean Sun were two to four times higher (54). These EUV fluxes easily compensate for lack of O<sub>2</sub> based on detailed calculations of the thermospheric temperature for an anoxic Earth (55). Greater pCO<sub>2</sub> could cool the thermosphere radiatively. The mesopause (the cold base of the thermosphere at about ~85-km altitude, where CO<sub>2</sub> cools radiatively) occurs at a pressure level inversely proportional to  $f_{CO_2}^{0.5}$ , where  $f_{CO_2}$  is the mixing ratio of CO<sub>2</sub> (56). At the upper pCO<sub>2</sub> limit (~0.04 bar) allowed by 2.75 Ga paleosols (27), the mesopause would be higher by only ~2 mesospheric scale heights (~10 km) in comparison to today. This altitude is still in the mixed region below the homopause, so diffusive separation in the overlying thermosphere would suppress thermospheric CO<sub>2</sub> abundances and prevent significant thermospheric cooling. The radiative cooling effects of molecular CH<sub>4</sub> on the thermopause can be neglected because CH<sub>4</sub> is photolyzed at lower altitudes (~60 km) and does not reach the thermosphere in a molecular form. So the idea of a cold Archean exobase is unsupported. Equally important, temperature-dependent Jean's escape is a minor process, on average. Nonthermal processes account for 60 to 90% of the H depopulation from the exobase (26, 27) and are intimately associated with the Earth's magnetic field. Thus, upward diffusion of H rather than the rate of H depopulation would set the Archean H escape rate from the exobase.

29. H. D. Holland, in (7), p. 83.  
 30. J. F. Kasting, D. H. Egger, S. P. Raeburn, *J. Geol.* **101**, 245 (1993).  
 31. The oxygen fugacity (fO<sub>2</sub>) of the upper mantle does not appear to have changed by more than 0.5 log<sub>10</sub> units since 3.6 Ga, based on redox-sensitive vanadium and chromium contents in igneous rocks (46, 39). These data contradict the hypothesis that a change in redox state of high-temperature volcanic gases facilitated the rise of O<sub>2</sub> (30, 32). Mantle fO<sub>2</sub> can remain constant even with continual net subduction of oxidized species, such as Fe<sup>3+</sup>, into the mantle over geologic time because of oxygen-buffering assemblages. As long as the mantle's mineral assemblage possesses all of the minerals involved on both sides of the chemical buffering reaction, fO<sub>2</sub> will remain buffered by that assemblage.  
 32. L. R. Kump, J. F. Kasting, M. E. Barley, *Geochem. Geophys. Geosyst.* **2** (2001). Available at: <http://146.201.254.53/publicationsfinal/researchletters/2000GC000114/fs2000GC000114.html>.  
 33. D. J. Des Marais, *Science* **289**, 1703 (2000).  
 34. W. S. Fyfe, N. J. Price, A. B. Thomson, *Fluids in the Earth's Crust* (Elsevier, New York, 1978), chap. 7.  
 35. Y. Shen, R. Buick, D. E. Canfield, *Nature* **410**, 77 (2001).  
 36. C. Lécuyer, Y. Ricard, *Earth Planet. Sci. Lett.* **165**, 197 (1999).  
 37. The redox state of metamorphic gases (i.e., gases that are not associated with a melt) is controlled by rock chemistry. Redox reactions in many metamorphosed crustal rocks are buffered by ferrous or ferric iron, carbon, or sulfur (34). For a given rock buffer, e.g., fayalite-magnetite-quartz (FMQ), low-temperature metamorphic gases tend to be more reducing (with more H<sub>2</sub>, CO, etc.) than their volcanic counterparts released at FMQ. When enough oxygen is added to crustal rocks to exhaust buffers, metamorphic gases increase in oxidation state by orders of magnitude. Redox balance requires that the overall oxidation state of metamorphic gases and the metamorphosed rocks they leave behind be preserved. Because the whole sedimentary rock reservoir is recycled with a half-life ~200 My even at present-day erosion rates (57), if O<sub>2</sub> were added to Archean sediments and associated crustal rocks, this would have inevitably created a more oxidized overall combination of

metamorphic gas and riverine weathering fluxes.  
 38. H. P. Eugster, *Proc. Internat. Geol. Congr.* **24** (no. 10), 3 (1972).  
 39. J. W. Delano, *Origin Life Evol. Biosphere*, in press.  
 40. M. Schidlowski, *Annu. Rev. Earth Planet. Sci.* **15**, 47 (1987).  
 41. Because of isotopic exchange of old rocks with recent waters, δD of the Archean oceans is poorly constrained [δD is the ratio of deuterium to hydrogen relative to the standard [2D/1H (standard)] for standard mean ocean water (SMOW), expressed in parts per thousand. δD = {[2D/1H (sample) - 2D/1H (standard)]/[2D/1H (standard)]} × 1000]. Kerogen δD, for example, is especially unreliable. However, Archean gneisses and granites from Swaziland have δD ~30 per mil (‰) lower than in Phanerozoic batholiths, which has proved puzzling (58). This might be explained if oceanic crust reacted with an ocean with a δD value closer to -30‰ rather than the present-day value of 0‰ (59). Methanogen methane has δD = -150 to -300‰. If oxygenic photosynthesis coupled to CH<sub>4</sub>-induced H escape caused cumulative oxidation ~2.5 × 10<sup>21</sup> mol O<sub>2</sub> (see Fig. 1B), 6.3% of the ancient ocean mass would have been lost. In the first approximation that D and H escape according to their proportions in biogenic methane, oceanic δD would increase ~10 to 20‰. Also, any tendency for the lighter H isotope to escape preferentially would further increase δD.  
 42. R. Rye, H. D. Holland, *Am. J. Sci.* **298**, 621 (1998).  
 43. M. Bau, R. L. Romer, V. Luders, N. J. Beukes, *Earth Planet. Sci. Lett.* **174**, 43 (1999).  
 44. N. Prasad, S. M. Roscoe, *Catena* **27**, 105 (1996).  
 45. J. Farquhar, H. Bao, M. Thiemens, *Science* **289**, 756 (2000).  
 46. D. Canil, *Geochim. Cosmo. Acta* **63**, 557 (1999).

47. D. J. Des Marais, H. Strauss, R. E. Summons, J. M. Hayes, *Nature* **359**, 605 (1992).  
 48. M. G. Green, P. J. Sylvester, R. Buick, *Tectonophysics* **322**, 69 (2000).  
 49. V. A. Melezhik, A. E. Fallick, P. V. Medvedev, V. V. Makarikhin, *Earth Sci. Rev.* **48**, 71 (1999).  
 50. R. A. Berner et al., *Science* **287**, 1630 (2000).  
 51. H. D. Holland, in (7), p. 388.  
 52. L. M. Francois, J. G. Gerard, *Paleoceanogr.* **1**, 335 (1986).  
 53. H. D. Holland, in (6), p. 284.  
 54. F. M. Walter, D. C. Berry, in *The Sun in Time*, C. P. Sonnett et al., Eds. (Univ. of Arizona Press, Tucson, 1991), pp. 633-657.  
 55. G. Visconti, *J. Atmos. Sci.* **32**, 1631 (1975).  
 56. J. W. Chamberlain, D. M. Hunten, *Theory of Planetary Atmospheres* (Academic Press, New York, 1987), pp. 34-36.  
 57. H. D. Holland, in (6), pp. 277-278.  
 58. H. P. Taylor, *J. Geol. Soc. London* **133**, 509 (1977).  
 59. C. Lécuyer, P. Gillet, F. Robert, *Chem. Geol.* **145**, 249 (1998).  
 60. R. A. Berner, D. E. Canfield, *Am. J. Sci.* **289**, 333 (1989).  
 61. M. I. Budyko, A. B. Ronov, A. L. Yanshin, *History of the Earth's Atmosphere* (Springer-Verlag, New York, 1985).  
 62. K. H. Wedepohl, *Geochim. Cosmochim. Acta* **59**, 1217 (1995).  
 63. A. D. Anbar, K. J. Zahnle, G. L. Arnold, S. J. Mojzsis, *J. Geophys. Res.* **106**, 3219 (2001).  
 64. We thank (in alphabetical order) B. Berner, R. Buick, D. DesMarais, J. Kasting, and E. Nisbet for discussion of this research over the last year. This work was funded by the NASA Exobiology and Astrobiology Programs.

25 April 2001; accepted 20 June 2001

## Josephson Junction Arrays with Bose-Einstein Condensates

F. S. Cataliotti,<sup>1,2,3</sup> S. Burger,<sup>1,2</sup> C. Fort,<sup>1,2</sup> P. Maddaloni,<sup>1,2,4</sup> F. Minardi,<sup>1,2</sup> A. Trombettoni,<sup>2,5</sup> A. Smerzi,<sup>2,5</sup> M. Inguscio<sup>1,2,3\*</sup>

We report on the direct observation of an oscillating atomic current in a one-dimensional array of Josephson junctions realized with an atomic Bose-Einstein condensate. The array is created by a laser standing wave, with the condensates trapped in the valleys of the periodic potential and weakly coupled by the interwell barriers. The coherence of multiple tunneling between adjacent wells is continuously probed by atomic interference. The square of the small-amplitude oscillation frequency is proportional to the microscopic tunneling rate of each condensate through the barriers and provides a direct measurement of the Josephson critical current as a function of the intermediate barrier heights. Our superfluid array may allow investigation of phenomena so far inaccessible to superconducting Josephson junctions and lays a bridge between the condensate dynamics and the physics of discrete nonlinear media.

The existence of a Josephson current through a potential barrier between two superconductors or between two superfluids is a direct manifesta-

tion of macroscopic quantum phase coherence (1, 2). The first experimental evidence of a current-phase relation was observed in superconducting systems soon after the Josephson effect was proposed in 1962 (3), whereas verification in superfluid helium has been presented only recently owing to the difficulty of creating weak links in a neutral quantum liquid (4, 5). The experimental realization of Bose-Einstein condensates (BEC) of weakly interacting alkali atoms (6, 7) has provided a route to study neutral superfluids in a controlled and tunable environment (8, 9) and to implement novel

<sup>1</sup>European Laboratory for Non-Linear Spectroscopy (LENL) and <sup>2</sup>Istituto Nazionale per la Fisica della Materia (INFM), Lgo E. Fermi 2, I-50125 Firenze, Italy. <sup>3</sup>Dipartimento di Fisica, Università di Firenze, Lgo E. Fermi 2, I-50125 Firenze, Italy. <sup>4</sup>Dipartimento di Fisica, Università di Padova, via F. Marzolo 8, I-35131 Padova, Italy. <sup>5</sup>International School for Advanced Studies (SISSA), via Beirut 2/4, I-34014 Trieste, Italy.

\*To whom correspondence should be addressed. E-mail: [inguscio@lens.unific.it](mailto:inguscio@lens.unific.it)

geometries for the connection of several Josephson junctions so far unattainable in charged systems. The possibility of loading a BEC in a one-dimensional periodic potential has allowed the observation of quantum phase effects on a macroscopic scale such as quantum interference (10) and the study of superfluidity on a local scale (11).

A Josephson junction (JJ) is a simple device made of two coupled macroscopic quantum fluids (2). If the coupling is weak enough, an atomic mass current  $I$  flows across the two systems, driven by their relative phase  $\Delta\phi$  as

$$I = I_c \sin \Delta\phi \quad (1)$$

where  $I_c$  is the "Josephson critical current," namely the maximal current allowed to flow through the junction. The relative phase dynamics, on the other hand, is sensitive to the external and internal forces driving the system:

$$\hbar \frac{d}{dt} \Delta\phi = \Delta V \quad (2)$$

where  $\hbar$  is Planck's constant divided by  $2\pi$ ,  $t$  is time, and  $\Delta V$  is the chemical potential difference between the two quantum fluids. Arrays of JJs are made of several simple junctions connected in various geometrical configurations. In the past decade, such systems have attracted much interest, because of their potential for studying quantum phase transitions in systems where the external parameters can be readily tuned (12). Recently, the creation of simple quantum-logic units and more complex quantum computer schemes (13) has been discussed. A great level of accuracy has been reached in the realization of two- and three-dimensional superconducting JJ arrays (12). One-dimensional (1D) geometries are more difficult to realize, because of the unavoidable presence of on-site frustration charges that substantially modify the ideal phase diagram. 1D JJ arrays with neutral superfluids (such as BEC), on the other hand, can be accurately tailored and open the possibility of directly observing several remarkable phenomena not accessible to other systems (14). First experiments with BECs held in a vertical optical lattice have shown the spatial and temporal coherence of condensate waves emitted at different heights of the gravitational field (10). More recently, the degree of phase coherence among different sites of the array (15) has been explored in the BEC ground state configuration.

We report on the realization of a 1D array of JJs by loading a BEC into an optical lattice potential generated by a standing-wave laser field. The current-phase dynamics, driven by an external harmonic oscillator potential provided by an external magnetic field, maps on a pendulumlike equation, and we performed a

measurement of the critical Josephson current as a function of the interwell potentials created by the light field.

The experimental apparatus has been described in detail elsewhere (11). We produce BECs of  $^{87}\text{Rb}$  atoms in the Zeeman state  $m_F = -1$  of the hyperfine level  $F = 1$  state confined by a cylindrically symmetric harmonic magnetic trap and a blue detuned laser standing wave, superimposed on the axis of the magnetic trap. In essence, the cylindrical magnetic trap is divided into an array of disk-shaped traps by the light standing wave. The axial and radial frequencies of the magnetic trap are  $\omega_x = 2\pi \times 9$  Hz and  $\omega_r = 2\pi \times 92$  Hz, respectively. By varying the intensity of the superimposed laser beam (detuned 150 GHz to the blue of the D1 transition at  $\lambda = 795$  nm) up to 14 mW/mm<sup>2</sup>, we can vary the interwell barrier energy  $V_0$  from 0 to  $5E_R$ , where  $E_R = \hbar^2/2m\lambda^2$  is the recoil energy of an atom (of mass  $m$ ) absorbing one of the lattice photons (16). The BEC is prepared by loading  $\sim 5 \times 10^8$  atoms in the magnetic trap and cooling the sample through radio-frequency-forced evaporation until a substantial fraction of condensed atoms is produced. We then switch on the laser standing wave and continue the evaporation ramp until no thermal component is experimentally visible. This ensures that the system reaches the ground state of the combined trap. The BEC splits in the wells of the optical array: The distance between the wells is  $\lambda/2$  and  $\sim 200$  wells are typically occupied, with  $\sim 1000$  atoms in each well. The interwell barrier energy  $V_0$ , and therefore the tunneling rate, are controlled by varying the intensity of the laser, which is chosen to be much higher than the condensate chemical potential  $\mu$ .  $\mu$  ranges between  $\mu \approx 0.10 V_0$  for  $V_0 = 2E_R$  and  $\mu \approx 0.04 V_0$  for  $V_0 = 5E_R$ . Each couple of condensates in neighboring wells therefore realizes a bosonic JJ, with a critical current  $I_c$  depending on the laser intensity.

In a more formal way, we can decompose the condensate order parameter that depends on position  $\vec{r}$  and time  $t$  as a sum of wave functions localized in each well of the periodic potential (tight binding approximation):

$$\Psi(\vec{r}, t) = \sqrt{N_T} \sum_j \psi_j(t) \Phi_j(\vec{r}) \quad (3)$$

where  $N_T$  is the total number of atoms and  $\psi_j = \sqrt{n_j(t)} e^{i\phi_j(t)}$  is the  $j$ th amplitude, with the fractional population  $n_j = N_j/N_T$  and the number of particles  $N_j$  and the phase  $\phi_j$  in the trap  $j$ . This assumption relies on the fact that the height of the interwell barriers is much higher than the chemical potential. We will show by a variational calculation that this assumption is verified in most of the range of our experimental parameters (17). The wave

function  $\Phi_j(\vec{r})$  of the condensate in the  $j$ th site of the array overlaps in the barrier region with the wave functions  $\Phi_{j\pm 1}$  of the condensates in the neighbor sites. Therefore, the system realizes an array of weakly coupled condensates, whose equation of motion satisfies a discrete nonlinear Schrödinger equation (18):

$$i\hbar \frac{\partial \psi_n}{\partial t} = -K(\psi_{n-1} + \psi_{n+1}) + (\epsilon_n + U|\psi_n|^2)\psi_n \quad (4)$$

where  $\epsilon_n = \Omega n^2$ ,  $\Omega = (1/2)m\omega_x^2(\lambda/2)^2 = 1.54 \times 10^{-5} E_R$  and  $U = g_0 N_T \int d\vec{r} \Phi_j^4$ . The tunneling rate is proportional to  $K \approx -\int d\vec{r} [(\hbar^2/2m)\nabla\Phi_j \cdot \nabla\Phi_{j+1} + \Phi_j V_{\text{ext}} \Phi_{j+1}]$ . A simple variational estimate, assuming a gaussian profile for the condensates in each trap, gives for  $V_0 = 3E_R$  the values  $K \sim 0.07E_R$ ,  $U \sim 12E_R$ , and a chemical potential  $\mu \sim 0.06V_0$  that is much lower than the interwell potential  $V_0$ . We observe that the wave functions  $\Phi_j$ , as well as  $K$ , depend on the height of the energy barrier  $V_0$ .

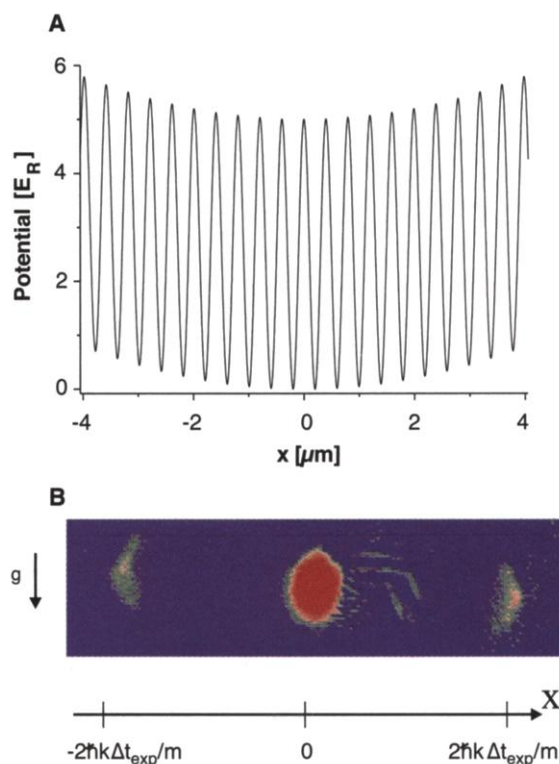
Equation 4 is a discrete nonlinear Schrödinger equation (DNLSE) in a parabolic external potential, conserving both the Hamiltonian  $\mathcal{H} = \sum_j [-K(\psi_j \psi_{j+1}^* + \psi_j^* \psi_{j+1}) + \epsilon_j |\psi_j|^2 + (U/2)|\psi_j|^4]$  and the norm  $\sum_j n_j = 1$ .

Although we can approximate the condensates in each lattice site as having their own wave functions, tunneling between adjacent wells locks all the different condensates in phase. As a result, when the condensates are released from the combined trap, they will show an interference pattern. This pattern consists of a central peak plus a symmetric comb of equally spaced peaks separated by  $\pm 2\hbar k_l t_{\text{exp}}/m$ , where  $k_l$  is the wave vector of the trapping laser and  $t_{\text{exp}}$  is the expansion time. In practice, one can think of the far field intensity distribution of a linear array of dipole antennas all emitting with the same phase. A complementary point of view is to regard the density distribution after expansion as the Fourier transform of the trapped one, i.e., the momentum distribution (19). It is easy to show that the sum of De Broglie waves corresponding to momentum states integer multiples of  $\pm 2\hbar k_l$  is the sum of localized wave functions of Eq. 3. The expanded cloud density distribution (Fig. 1) consists of three distinct atomic clouds spaced by  $\sim 306 \mu\text{m} \approx 2\hbar k_l t_{\text{exp}}/m$ , with the two external clouds corresponding to the first-order interference peaks, each containing roughly 10% of the total number of atoms. The interference pattern therefore provides us with information about the relative phase of the different condensates (15, 20); indeed, by repeating the experiment with thermal clouds, even with a temperature considerably lower than the interwell potential, we did not observe the interference pattern.

This situation is different from the Bragg diffraction of a condensate released from a harmonic magnetic trap (21) where the condensate is diffracted by a laser standing wave. In our case, it is the ground state of the combined magnetic harmonic trap plus optical periodic potential that by expansion produces an interference pattern. For the time scales of our experiment, the relative intensities of the three interference peaks do not depend on the time the atoms spend in the optical potential, indicating that the steady state of the system has been reached. In absence of external perturbations, the condensate remains in the state described by Eq. 3 with a lifetime of  $\sim 0.3$  s at the maximum light power, limited by scattering of light from the laser standing wave.

In the ground state configuration, the BECs are distributed among the sites at the bottom of the parabolic trap. If we suddenly displace the magnetic trap along the lattice axis by a small distance of  $\sim 30$   $\mu\text{m}$  (the dimension of the array is  $\sim 100$   $\mu\text{m}$ ), the cloud will be out of equilibrium and will start to move. As the potential energy that we give to the cloud is still smaller than the interwell barrier, each condensate can move along the magnetic field only by tunneling through the barriers. A collective motion can only be established at the price of an overall phase coherence among the condensates. In other words, the relative phases among all adjacent sites should remain locked together to preserve the ordering of the collective motion. The locking of the relative phases will again show up in the expanded cloud interferogram.

**Fig. 1. (A)** Combined potential of the optical lattice and the magnetic trap in the axial direction. The curvature of the magnetic potential is exaggerated by a factor of 100 for clarity. **(B)** Absorption image of the BEC released from the combined trap. The expansion time was 26.5 ms and the optical potential height was  $5E_R$ .



For displacements that are not very large, we observe a coherent collective oscillation of the condensates; i.e., we see the three peaks of the interferogram of the expanded condensates oscillating in phase, thus showing that the quantum mechanical phase is maintained over the entire condensate (Fig. 2). In Fig. 2A, we show the positions of the three peaks as a function of time spent in the combined trap after the displacement of the magnetic trap, compared with the motion of the condensate in the same displaced magnetic trap but in the absence of the optical standing wave (we refer to this as “harmonic” oscillation). The motion performed by the center of mass of the condensate is an undamped oscillation at a substantially lower frequency than in the “harmonic” case. We will comment on this frequency shift later in the text; we would like now to further stress the coherent nature of the oscillation. To do so, we repeat the same experiment with a thermal cloud. In this case, although individual atoms are allowed to tunnel through the barriers, no macroscopic phase is present in the cloud and no motion of the center of mass should be observed. The center of mass positions of the thermal clouds are reported in Fig. 2B together with the “harmonic” oscillation of the same cloud in the absence of the optical potential. As can be seen, the thermal cloud does not move from its original position in the presence of the optical lattice. Indeed, if a mixed cloud is used, only the condensate fraction starts to oscillate while the thermal component remains static, with the interaction of the two eventually leading to a damping of the condensate motion.

We now turn back to the discussion of the frequency reduction observed in the oscillation of the pure condensate in the presence of the optical lattice. The current flowing through the junction between two quantum fluids has a maximum value, the critical Josephson current  $I_c$ , which is directly proportional to the tunneling rate. The existence of such a condition essentially limits the maximum velocity at which the condensate can flow through the interwell barriers and therefore reduces the frequency of the oscillations. As a consequence, we expect a dependence of the oscillation frequency on the optical potential through the tunneling rate.

To formalize the above reasoning, we rewrite the DNLS (Eq. 4) in terms of the canonically conjugate population/phase variables, therefore enlightening its equivalence with the Josephson equations for a 1D junction array:

$$\hbar \dot{n}_j = 2K \sqrt{n_j n_{j-1}} \sin(\phi_j - \phi_{j-1}) - 2K \sqrt{n_j n_{j+1}} \sin(\phi_{j+1} - \phi_j) \quad (5a)$$

$$\hbar \dot{\phi}_j = -Un_j - \Omega_j^2 + K \sqrt{n_{j-1}/n_j} \cos(\phi_j - \phi_{j-1}) + K \sqrt{n_{j+1}/n_j} \cos(\phi_{j+1} - \phi_j) \quad (5b)$$

It is useful to introduce collective coordinates (18): The center of mass  $\xi(t)$  and the dispersion  $\sigma(t)$  are defined, respectively, as  $\xi(t) = \sum_j n_j$

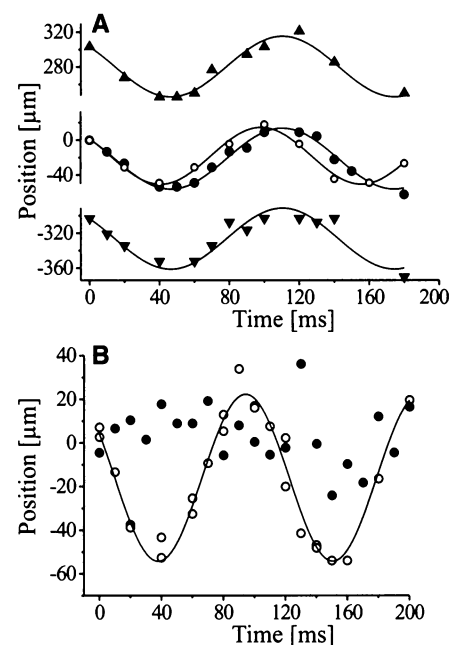
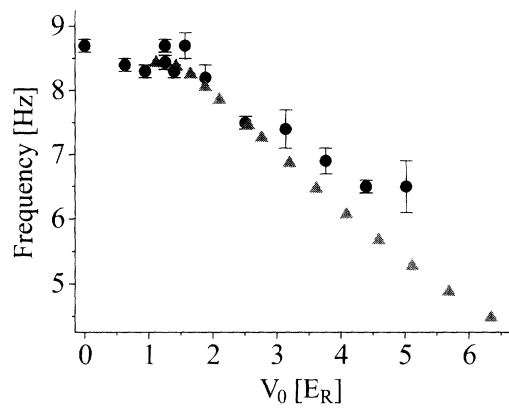


**Fig. 2. (A)** Center of mass positions of the three peaks in the interferogram of the expanded condensate as a function of the time spent in the combined trap after displacement of the magnetic field. Up and down triangles correspond to the first-order peaks; filled circles correspond to the central peak. Open circles show the center of mass position of the BEC in the absence of the optical lattice. The continuous lines are the fits to the data. **(B)** Center of mass positions of the thermal cloud as a function of time spent in the displaced magnetic trap with the standing wave turned on (filled circles) and off (open circles).

**Fig. 3.** The frequency of the atomic current in the array of Josephson junctions as a function of the interwell potential height. Experimental data (circles) are compared with the calculated values (triangles). Each experimental data point was taken after a complete oscillation in the displaced magnetic trap. The oscillation was then fitted with a sine function giving the corresponding frequency (error bars are the standard deviation of the data from the fit).



and  $\sigma^2(t) = \sum_j n_j - \xi^2$ . From Eqs. 5a and 5b, we have  $\hbar \dot{\xi} = 2K \sum_j \sqrt{n_j n_{j+1}} \sin(\phi_{j+1} - \phi_j)$ . As the number of atoms is large, the “kinetic” energy term of DNLS is small with respect to the potential and nonlinear terms, and the population density profile is simply given by an inverted discrete parabolic profile, centered around  $\xi$  (22):  $n_j(t) = [\mu - \Omega(j - \xi)^2]/U$ ; furthermore,  $(d/dt)\sigma^2 = 0$ .

During the dynamical evolution, the relative phases across the junctions  $\phi_{j+1} - \phi_j \equiv \Delta\phi(t)$  remain locked together to the same (oscillating) value. This has been verified by numerically studying the Fourier transform  $\tilde{\psi}_k = \sum_j \psi_j e^{ikj}$ ; from the experimental point of view, this means that the expanded condensate continues to show the three peaks of the interferogram of Fig. 1. Therefore in these collective coordinates the current-phase relation is given by

$$\hbar \frac{d}{dt} \xi(t) = 2K \sin \Delta\phi(t) \quad (6a)$$

$$\hbar \frac{d}{dt} \Delta\phi(t) = -m\omega_x^2 \left(\frac{\lambda}{2}\right)^2 \xi(t) \quad (6b)$$

which, in analogy with the case of a superconducting Josephson junction [in the resistively shunted junction model (1, 2)] and with the case of  $^3\text{He}$  (5), is a pendulum equation with the relative phase  $\Delta\phi$  corresponding to the angle to a vertical axis and the center of mass  $\xi$  being the corresponding angular momentum. The current-phase dynamics does not depend explicitly on the interatomic interaction. This allows us to study regimes with a number of condensate atoms spanning over different orders of magnitude, which is different from the configuration considered in (10) where nonlinear effects would dephase the collective dynamics. However, it is clear that the nonlinear interaction is crucial to determining the superfluid nature of the coupled condensates, by locking the overall phase coherence against perturbations.

From Eqs. 6a and 6b, we can see that the small-amplitude oscillation frequency  $\omega$ , of the current  $I \equiv N_T(d/dt)\xi$  gives a direct measurement of the critical Josephson current  $I_c \equiv 2KN_T/\hbar$  and, therefore, of the atomic tunneling

rate of each condensate through the barriers. The critical current is related to the frequency  $\omega$  of the atomic oscillations in the lattice and to the frequency  $\omega_x$  of the condensate oscillations in the absence of the periodic field by the relation

$$I_c = \frac{4\hbar N_T}{m\lambda^2} \left(\frac{\omega}{\omega_x}\right)^2 \quad (7)$$

Figure 3 shows the experimental values of the oscillation frequencies together with the result of a variational calculation based on Eqs. 5a and 5b. It must be noted that, because of mean field interactions, in our system a bound state exists in the lattice only for potentials higher than  $\sim E_R$ ; frequency shifts for lower potential heights are better explained in terms of the effective mass  $1/m_{\text{eff}} = \partial^2 \mathcal{E}/\partial k^2$  of the system (11).

Increasing the initial angular momentum  $\xi_0$ , the pendulum librations become anharmonic and can eventually reach the value  $\Delta\phi_{\text{max}} = \pi/2$ . The system becomes dynamically unstable, and the phase coherence is lost after a transient time (the interference patterns wash out). In this regime, the pendulum analogy breaks down and a different dynamical picture would emerge.

With this work, we have verified that the BEC’s dynamics on a lattice is governed by a discrete, nonlinear Schrödinger equation. This equation is common to a large class of discrete nonlinear systems, including polarons, optical fibers, and biological molecules (23), thus opening up interdisciplinary research. The phase rigidity among different wells can be probed against thermal fluctuations to test various theories of decoherence (24). One could study the role of collective dynamical modes in the creation of solitons and kinks of the type described in (18, 25, 26) [see also (23)] and more generally the routes to quantum phase transitions in nonhomogeneous, low-dimensional systems.

**References and Notes**

1. A. Barone, in *Quantum Mesoscopic Phenomena and Mesoscopic Devices in Microelectronics*, I. O. Kulik, R. Ellialtıoglu, Eds. (Kluwer Academic, Dordrecht, Netherlands, 2000), pp. 301–320.
2. ———, G. Paterno, *Physics and Applications of the Josephson Effect* (Wiley, New York, 1982).

3. B. D. Josephson, *Phys. Lett.* **1**, 251 (1962).
4. O. Avenel, E. Varoquaux, *Phys. Rev. Lett.* **60**, 416 (1988).
5. S. V. Pereverzev, S. Backaus, A. Loshak, J. C. Davis, R. E. Packard, *Nature* **388**, 449 (1997).
6. M. Inguscio, C. E. Wieman, S. Stringari, Eds., *Bose-Einstein Condensation in Atomic Gases* (IOS Press, Amsterdam, 1999).
7. S. Martellucci, A. N. Chester, A. Aspect, M. Inguscio, Eds., *Bose-Einstein Condensates and Atom Lasers* (Kluwer Academic/Plenum, New York, 2000).
8. F. Dalfovo, S. Giorgini, L. P. Pitaevskii, S. Stringari, *Rev. Mod. Phys.* **71**, 463 (1999).
9. A. J. Leggett, *Rev. Mod. Phys.* **73**, 307 (2001).
10. B. P. Anderson, M. A. Kasevich, *Science* **282**, 1686 (1998).
11. S. Burger *et al.*, *Phys. Rev. Lett.* **86**, 4447 (2001).
12. R. Fazio, H. van der Zant, *Phys. Rep.*, in press (preprint available at xxx.lanl.gov/abs/cond-mat/0011152).
13. Y. Makhlin, G. Schön, A. Shnirman, *Rev. Mod. Phys.* **73**, 357 (2001).
14. A. Smerzi, S. Fantoni, S. Giovannazzi, S. R. Shenoy, *Phys. Rev. Lett.* **79**, 4950 (1997).
15. C. Orzel, A. K. Tuchman, M. L. Fenselau, M. Yasuda, M. A. Kasevich, *Science* **291**, 2386 (2001).
16. The value of the optical potential used in all the variational calculations was calibrated by performing Bragg diffraction experiments on the BEC released from the harmonic trap. The experimental result deviates from the potential calculated from the measured laser power mainly because of alignment imperfections.
17. The validity of the tight binding approximation is also based on the fact that the tunneling of atoms in the higher energy band is energetically forbidden: Because the gap is  $\sim 3E_R$ , the potential energy  $(1/2)m\omega_x^2(\lambda/2)^2 j^2$  for that would require  $j \sim 500$ , i.e., displacements three times larger than the condensate dimensions.
18. A. Trombettoni, A. Smerzi, *Phys. Rev. Lett.* **86**, 2353 (2001).
19. The expanded density distribution reproduces the momentum distribution for expansion times much longer than the inverse of the trapping frequencies if the nonlinear terms in the Schrödinger equations (the mean field) can be neglected during the expansion. The trapping frequencies of the single traps in the array are on the order of a few kHz and the expansion time is 26.5 ms, so the first assumption is readily verified. The question of neglecting the mean field in the first part of the expansion when the density is still comparable to the original condensate is more delicate. However, this will only affect the shape of the single interference peaks and not the overall interference pattern.
20. M. Greiner, I. Bloch, O. Mandel, T. W. Haensch, T. Esslinger, preprint available at xxx.lanl.gov/abs/cond-mat/0105105.
21. M. Kozuma *et al.*, *Phys. Rev. Lett.* **82**, 871 (1999).
22. This is the discrete analog of the “Thomas-Fermi” approximation for the continuous Gross-Pitaevskii equation with an external parabolic potential. In this limit, as will be shown below, the dynamics does not depend explicitly on the nonlinear interatomic interaction, which only governs the overall shape. Our collective mode, indeed, can be seen as the discrete analog of the dipole mode in the continuous Gross-Pitaevskii equation, whose frequency depends only on the parameters of the external harmonic trap.
23. A. C. Scott, *Nonlinear Science: Emergence and Dynamics of Coherent Structures* (Oxford Univ. Press, Oxford, 1999).
24. W. Zurek, *Phys. Today* **44**, 36 (1991).
25. A. Sanchez, A. R. Bishop, *SIAM Rev.* **40**, 579 (1998).
26. F. Kh. Abdullaev, B. B. Baizakov, S. A. Darmanyan, V. V. Konotop, M. Salerno, *Phys. Rev. A*, in press (preprint available at xxx.lanl.gov/abs/cond-mat/0106042).
27. This work has been supported by the Cofinanziamento Ministero dell’Università e della Ricerca Scientifica e Tecnologica, by the European Community under contract HPRI-CT-1999-00111 and HPRN-CT-2000-00125, and by the Istituto Nazionale per la Fisica della Materia Progetto di Ricerca Avanzata “Photonmatter.” We thank M. Kasevich and S. Stringari for helpful discussions. A.S. and A.T. wish to thank the LENS for the kind hospitality during the realization of this work.

17 May 2001; accepted 29 June 2001